View metadata, citation and similar papers at
brought to you by CORE
provided by Utrecht University Repository

How amoeboids self-organize into a fruiting body: Multicellular coordination in *Dictyostelium discoideum*

Athanasius F. M. Marée* and Paulien Hogeweg

Theoretical Biology and Bioinformatics, University of Utrecht, Padualaan 8, 3584 CH Utrecht, The Netherlands

Edited by J. T. Bonner, Princeton University, Princeton, NJ, and approved January 22, 2001 (received for review November 9, 2000)

When individual amoebae of the cellular slime mold *Dictyostelium discoideum* are starving, they aggregate to form a multicellular migrating slug, which moves toward a region suitable for culmination. The culmination of the morphogenesis involves complex cell movements that transform a mound of cells into a globule of spores on a slender stalk. The movement has been likened to a "reverse fountain," whereby prestalk cells in the upper part form a stalk that moves downwards and anchors to the substratum, while prespore cells in the lower part move upwards to form the spore head. So far, however, no satisfactory explanation has been produced for this process. Using a computer simulation that we developed, we now demonstrate that the processes that are essential during the earlier stages of the morphogenesis are in fact sufficient to produce the dynamics of the culmination stage. These processes are cAMP signaling, differential adhesion, cell differentiation, and production of extracellular matrix. Our model clarifies the processes that generate the observed cell movements. More specifically, we show that periodic upward movements, caused by chemotactic motion, are essential for successful culmination, because the pressure waves they induce squeeze the stalk downwards through the cell mass. The mechanisms revealed by our model have a number of self-organizing and self-correcting properties and can account for many previously unconnected and unexplained experimental observations.

When their bacterial food source is depleted, individual amoebae of the cellular slime mold *Dictyostelium discoideum* aggregate to form a multicellular migratory slug, which is surrounded by a slime sheath. The slug has phototactic and thermotactic properties, which direct it to a suitable site for culmination. When it finds a good location or when time is running out, migration halts and in about four hours a fruiting body is formed; the fruiting body has a stalk that supports a spore head elevated above the substratum to facilitate spore dispersal.

We have modeled the process of culmination by using a hybrid stochastic cellular automata (CA)/partial differential equation model (1–3). Individual cells are modeled as a group of connected automata—i.e., the basic scale of the model is subcellular. Our model is an extension of the Glazier and Graner model formalism (4), in which cell displacements are driven by differential cell adhesions, combined with a sloppy volume conservation. We have added the following properties: cAMP signaling, chemotaxis, cell differentiation, and rigidity.

Entirely based on these processes, we propose a new mechanism for the complex morphogenetic movements, and we show that the mechanism is indeed sufficient to produce the fruiting body. By periodic upward movements of the cells, caused by a combination of chemotactic motion and adhesion, pressure waves are induced that squeeze the stalk downwards through the cell mass.

Our model is based on the following experimental observations. Periodic cell movements occur during aggregation and slug migration (5), as well as during culmination (6). Although the movement mechanisms are still under debate (7), there is increasing experimental evidence that the coordinated upward movement of the cells is organized by a combination of a pulsatile cAMP excretion and a cAMP-mediated cAMP response, accompanied by a chemotactic response to the cAMP (8). The cAMP waves originate in the prestalk A (PstA) region, which is located in the uppermost part of the culminant. Then the cAMP signal is relayed by prestalk O (PstO) cells, which occupy the posterior part of the prestalk zone, and by prespore cells, which occupy the lower part of the culminant (9, 10). Not only cAMP, but also cell–cell adhesion and cell–substratum adhesion play an important role in regulating cell movements (11, 12). Moreover, the culminant is surrounded by an extracellular matrix, called the slime sheath, which also functions in the motility of the organism (13).

During culmination a unidirectional conversion of cell types takes place: PstO cells differentiate into PstA cells, and PstA cells into stalk cells (14, 15). We assume that contact between the cell types is required for this process, because cell induction has not been detected even at a distance of a few cell diameters (9). The newly created stalk cells produce a stiff extracellular matrix (16) and increase their volume by vacuolation (17).

A special group of cells, which first appear during the slug stage (16), occupies the tip region of the downward-elongating stalk (14). Because of their position and the fact that the stalk elongates straight downwards, these cells are assumed to guide the elongation; they are therefore referred to as pathfinder cells (16). Although the symmetry in upward and downward motion is striking, neither stalk cells nor pathfinder cells respond to cAMP, and no other clue as to the stimulus directing the downward movement has been found (15). Hence in our model, pathfinder cells simply differ from stalk cells in adhesion strengths. We start our simulations when stalk cell differentiation has just begun and a small number of pathfinder cells are positioned at the stalk tip.

Description of the Model

In our model we have implemented only the above-mentioned experimentally elucidated mechanisms. We have modeled the culmination by using two-dimensional simulations, which are considered to be transverse sections. The plane is decomposed into a uniform grid, every square of which is regarded as a cellular automaton. We used the Glazier and Graner model (4) extended in the following way. Every cell is represented as a group of connected automata in the CA—i.e., each cell has a unique identification number, σ, which is assigned to all automata that form the amoeba. In our simulations, one cell occupies $\approx$30 automata in the CA. Each cell also has a type label τ, which

This paper was submitted directly (Track II) to the PNAS office.

Abbreviations: CA, cellular automata; PstA, prestalk A; PstO, prestalk O; Psp, prespore; St, stalk; Pf, pathfinder; Sl, slime sheath; Tu, stalk tube.

See commentary on page 3639.

*To whom reprint requests should be addressed. E-mail: S.Maree@bio.uu.nl.

The publication costs of this article were defrayed in part by page charge payment. This article must therefore be hereby marked "*advertisement*" in accordance with 18 U.S.C. §1734 solely to indicate this fact.

Table 1. Parameter settings used in the simulations

	J_{τ_1,τ_2}											
Cell type	Air	Soil	Psp	PstO	PstA	St	Pf	Sl	Tu	No. cells	V	cAMP
Psp	20	11	9							1,960	30	Relay
PstO	27	14	13	7						1,011	30	Relay
PstA	33	16	13	10	3					79	30	Oscillatory
St	43	20	25	24	16	3				25	30–40	Decay
Pf	35	8	10	10	17	7	11			14	30	Decay
Sl	5	7	8	15	21	21	7	—		1	3,000	Decay
Tu	5	9	10	11	12	3	5	1	—	1	3 × no. St	—

For each cell type the values of J_{τ_1,τ_2}, the initial number of cells, their target volume, V, and the type of cAMP dynamics (cAMP relay, oscillatory, or small decay) are shown. Other parameters used are $T = 6$, $\lambda = 1$, $\mu = 200$, $H_{\text{diss}} = 0.8$, $H_{\text{tubediss}} = 30$, and $\Delta t_{\text{induction}} = 8.5$ sec.

indicates whether the cell type is prespore, PstO, PstA, stalk, or pathfinder ($\tau \in \{\text{Psp, PstO, PstA, St, Pf}\}$). Between each pair of cell types dimensionless free energy bonds ($J_{\tau_1,\tau_2} > 0$) are defined, which describe the cell–cell and cell–substratum adhesion. The values of J_{τ_1,τ_2} as well as the other parameters used in the CA are given in Table 1. The total free energy of a cell is given by

$$H_\sigma = \sum \frac{J_{\text{type,type}}}{2} + \sum J_{\text{type,Air}} + \sum J_{\text{type,Soil}} + \lambda(v_\sigma - V)^2. \quad [1]$$

Because biological cells have a more or less fixed size, Glazier and Graner (4) added to the free energy function an extra term, to describe the area constraint for each individual cell. This term $\lambda(v_\sigma - V)^2$, where v_σ is the actual volume, V the target volume, and λ the inelasticity, ensures that the volume of a cell remains close to V. Minimization of the free energy causes boundary deformation. ΔH gives the change in free energy if a boundary deformation were to occur. The probability that a boundary will indeed be deformed is either 1 if $\Delta H < -H_{\text{diss}}$ or $\exp-[(\Delta H + H_{\text{diss}})/T]$ if $\Delta H \geq -H_{\text{diss}}$. H_{diss} represents the dissipation costs involved in deforming a boundary; T represents the default mobility of the cells.

The CA is used to describe not only the individual cells but also the extracellular matrix: to describe the slime sheath and the stalk tube ($\tau \in \{\text{Sl, Tu}\}$), two entities are defined which follow the same rules and can deform in the same way as all cells, which, however, have a much larger target volume. The stiffness of the stalk tube is described by a high H_{diss}. The slime sheath has a fixed target volume; the target volume of the stalk tube increases whenever a new stalk cell appears. Initially, the open space between the cells is filled with slime mass; the slime then spreads out over the cell mass, forming the slime sheath within a few time steps.

The induction of PstA cells into stalk cells is implemented by searching PstA–stalk cell contacts at fixed time intervals ($\Delta t_{\text{induction}}$). The chance of changing one PstA cell into a stalk cell is proportional to the amount of contact area. The differentiation of PstO cells into PstA cells is modeled in the same way. During the first 15 min after their appearance stalk cells increase their target volume by 33%.

To describe the cAMP dynamics we use discretized partial differential equations with the same grid size as the CA. The cAMP can diffuse freely through all cells and through the slime sheath, but neither through the tube, which is considered to be impermeable to cAMP, nor into the air or soil. Excitable cAMP dynamics can be described reasonably well in a quantitative way by two variable FitzHugh–Nagumo equations with piecewise linear "Pushchino kinetics" (18). For more background on the use of this model to describe the basic properties of cAMP signaling in *Dictyostelium*, see ref. 2. This description, which we have used for cell types Psp, PstO, and PstA, reproduces the overall characteristics of cAMP waves, such as oscillatory dynamics, cAMP relay, refractoriness, eikonal–curvature relation, etc. For the other cell types (St, Pf, and Sl) a small decay of cAMP is implemented.

Here we have used the same parameter settings to describe the cAMP dynamics as used previously (2). The partial differential equations are solved by the explicit Euler method (with time step equal to 0.01 and space step equal to 0.37). Table 1 also indicates which kinds of cAMP dynamics were used for the different cell types.

Provided their refractoriness is not too high, prespore and prestalk cells respond to the cAMP signal by making a chemotactic movement toward the cAMP. Chemotaxis is incorporated by using the local cAMP spatial gradient: $\Delta H' = \Delta H - \mu(\text{cAMP}_{\text{automaton}} - \text{cAMP}_{\text{neighbor}})$.

In the simulation of Fig. 4, all prestalk and prespore cells produce NH_3, which can also diffuse into the air. The inhibiting effect of NH_3 (n) on the cAMP dynamics is incorporated by increasing the value of parameter $a_{\tau,n}$, which defines the excitability of the cell (see ref. 3): $a(\tau, n) = a_\tau + b_\tau n^s/[1 + (n/p)^s]$, with $a_{\text{PstA}} = -0.20$, $a_{\text{PstO}} = a_{\text{Psp}} = -0.025$, $b_{\text{PstA}} = 0.0375$, $b_{\text{PstO}} = b_{\text{Psp}} = 0.075$, $p = 2$, $s = 3$; the parameters for production and diffusion of NH_3 are $R_n = 10^{-3}$ and $D_n = 15$.

Time and space are scaled so as to simulate realistic characteristics for the periodicity and signal propagation of the cAMP waves (19, 20). In each simulation step, every boundary CA is subjected to a possible change to a CA of the adjacent cell type, with a probability in terms of ΔH as described above. A simulation step corresponds to 0.1 sec and one grid interval corresponds to 5 μm.

MPEG movies of the simulations are available as supplemental web material at www.pnas.org.

Results

We now describe and explain the process of culmination as it unfolds in the model and refer to experiments in which comparable behavior has been observed. Fig. 1 shows that on a time scale consistent with experiments (21) a mound of cells develops into a fruiting body. As a result of the strong adhesion between the stalk cells and the much weaker adhesion between stalk and PstO cells, the stiff matrix produced by the stalk cells is "squeezed" outwards, where it accumulates at the boundary between the two cell types: very rapidly a stalk tube is formed (9). The top of the tube forms a gate through which prestalk cells can enter (17). The gate remains open as a result of the combined effect of ongoing induction, differential adhesion, and stiffness of the matrix. Periodically cAMP waves, originating in the PstA region, move downward through the cell mass. These waves, combined with the chemotactic response, lead to the upward cell motion (22).

Because of adhesion, the pathfinder cells immediately surround the stalk tip (16). Although neither the pathfinder cells

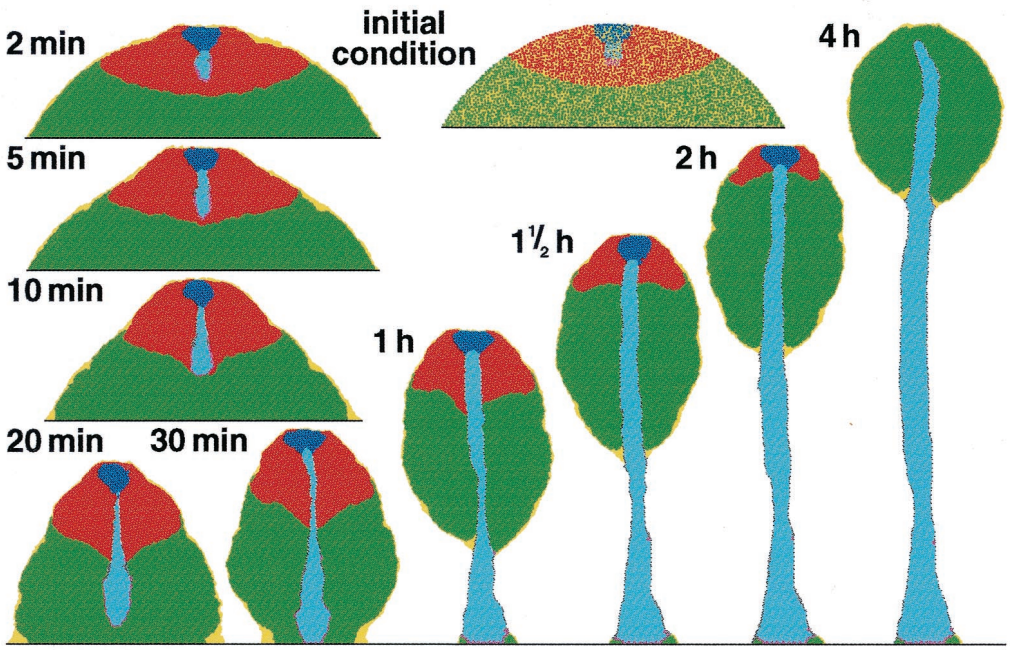

Fig. 1. Time sequence of a simulation of the process of culmination. The cell types are Psp (green), PstO (red), PstA (blue), St (cyan), Pf (magenta), Sl (yellow), and Tu (gray). The process is shown in MPEG Movie 1, which is published as supplemental data on the PNAS web site, www.pnas.org.

nor the stalk cells are chemotactic, the tip elongates downwards at a greater speed than the chemotactic upward motion. The stalk tip reaches the base around 20 min after entering the prespore region, which is just as fast as observed in experiments (14). The mechanism can be elucidated as follows (see Fig. 2).

Downward-moving cAMP waves periodically trigger an upward-directed chemotactic response. Because chemotactically moving cells push cells in front of them and pull cells that are behind them (because of cell adhesion), the equivalent of pressure differences are created. Therefore every cAMP wave is accompanied by a pressure wave. Moreover, because of cell adhesion, cells start moving before the cAMP wave arrives, because they are pulled toward the chemotactically moving amoebae. And when the cAMP wave has passed, cell motion continues for a while, because cells that are located just below keep on pushing the cells upwards. Hence the pressure waves are much broader than the cAMP waves, and upward motion is far more gradual, compared with the pulsatile cAMP signal. The pathfinder cells are pushed and pulled by these pressure waves, which results in a peristaltic motion of the stalk tip. The pathfinder cells, and along with them the stalk cells, are thereby squeezed downward. Newly recruited stalk cells are transported through the tube by the combination of pushing at the tube gate, attributable to the surface tension between PstA and stalk cells, and pulling at the stalk tip, attributable to the peristaltic motion.

Although an elongated shape moving against a flow has a very strong tendency to bend sideways, the mechanism revealed by our model very efficiently restores any such deviation. Fig. 3 shows that even if initially the stalk is bent 90°, it extends downward again after only 15 min. When the stalk tip is not precisely pointing downward, the cAMP waves reach one side earlier. Hence, the moment this side is pushed, the other side is still pulled. This force efficiently transports the cells inward, instead of downward, and restores the original orientation. Peristalsis also explains the position of the pathfinder cells. When more than half of the pathfinder cells happen to be

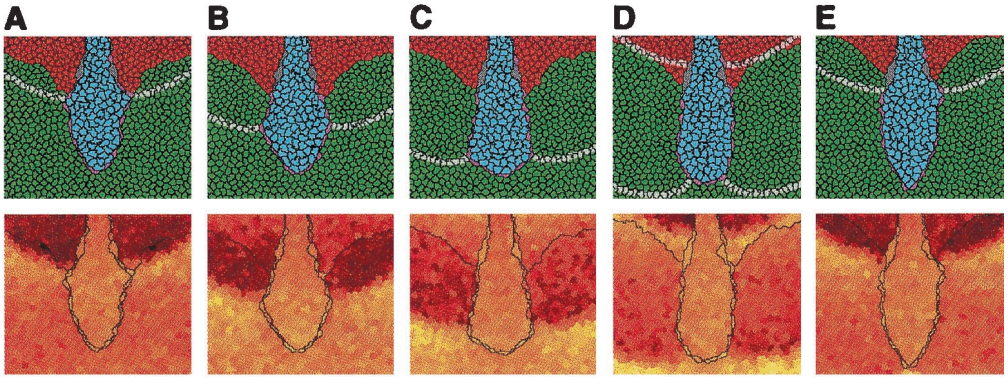

Fig. 2. Detailed view of the stalk elongation during the simulation of Fig. 1. (*Upper*) Individual cells. Light bands indicate the regions of chemotactic motion toward cAMP. See also Movie 2, which is published as supplemental data on the PNAS web site, www.pnas.org. (Lower) Pressure differences, indicated by the mean cell volume of individual cells, averaged over five samples at intervals of 2 sec. Volumes are indicated by a color gradient from dark red (small volume) to bright yellow (large volume). (*A*) At 14 min and 40 sec. (*B–E*) With subsequent intervals of 40 sec. See also Movie 3, which is published as supplemental data.

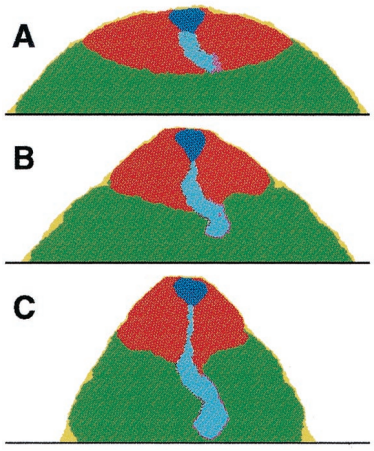

Fig. 3. Restoration of the direction of stalk elongation. Initially, the stalk tip is bent 90°. (*A*) 50 sec. (*B*) 8 min and 20 sec. (*C*) 16 min and 40 sec. See also Movie 4, which is published as supplemental data on the PNAS web site, www.pnas.org.

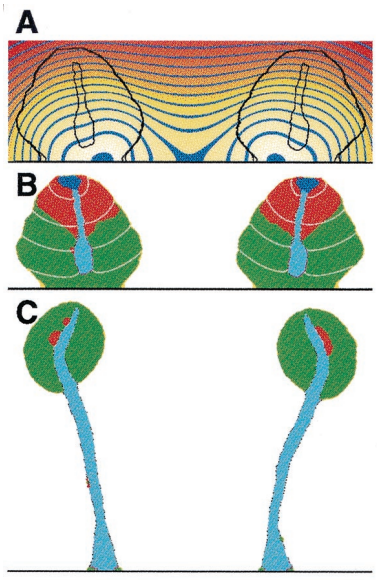

Fig. 4. Snapshot, after 20 min, of two culminants orienting away from each other because of NH_3 production. (*A*) NH_3 distribution, indicated by a color gradient from dark red (low concentration) to bright yellow (high concentration), with blue bands of iso-concentration. See also Movie 5, which is published as supplemental data on the PNAS web site, www.pnas.org. (*B*) The culminants, with slanted stalks. Light bands indicate the cAMP waves. (*C*) Final configuration after 4 h. See also Movie 6, which is published as supplemental data.

positioned along one side of the stalk, the imbalance is quickly rectified. This is because downward motion on the more crowded side is more efficient and pushes the cells back to the other side. Hence the pathfinder cells always remain positioned along the tip of the stalk, yet another property that is not explicitly incorporated in the model.

The downward motion stops automatically when the stalk tip reaches the base, because the tip is no longer completely surrounded by cAMP waves. The upward motion of the prespore cells also stops in a self-organizing way when the PstA cell type is depleted. The cAMP waves now also cease, because the PstA cells were the ones that periodically produced the cAMP signal. Therefore the upward motion halts at the moment the stalk formation is completed. After the chemotactic motion has stopped, the prespore cell mass becomes rounded, because of surface tension properties. The tube, however, is too stiff to change its general shape. Thus, in the model, a globule of spores on a slender stalk is the stable final configuration. The indirect mechanisms described here not only generate the normal culmination process but also are self-correcting and self-terminating. We therefore refute the claim in the literature that the stalk is pushed downwards as a result of the addition of stalk cells at the top (16, 23). Our model rules out this possibility.

Many other experimental observations are in agreement with our model. For example, when the differentiation of PstA cells into stalk cells is blocked, and hence no stalk is formed, in both model and experiments the culminant still moves upwards, but ends up as an erratic hair-like structure (24). In the model this behavior is due to upward motion by chemotaxis, which does not stop because the prestalk pool is never emptied. However, the results of this experiment cannot be reconciled with the classical view that the cells are pushed upward by the stalk elongation (16, 23). When the rate of chemotactic motion is reduced (22) or when upward motion is prevented by an extreme centrifugal force ($40–50 \times g$) (25), no normal stalk formation is observed. The simple explanation provided by the model is that periodic upward motion is necessary for the downward elongation. In experiments a constriction develops at the base of the prespore zone before the stalk reaches the substratum (26). In the model this is due to the combination of cellular adhesion and upward motion.

Finally, culminants orient away from NH_3 (27), as well as away from each other, apparently because they themselves produce NH_3 (28). Fig. 4 shows how this behavior can be accounted for: The cells produce a small quantity of NH_3, which inhibits the cAMP-induced cAMP release [by inhibiting the activation of adenylate cyclase (29)]; NH_3 accumulates between the two adjacent culminants, and because cAMP waves move more slowly at higher NH_3 concentrations, the waves become slanted. The stalks, which extend perpendicular to the cAMP waves, move toward each other instead of straight downward, and the fruiting bodies end up oriented away from each other.

Discussion

We have previously used the same model formalism, including the same processes of differential adhesion, cAMP signaling, and chemotaxis, to explain the aggregation of single amoebae into a mound and a moving slug (1), as well as to unravel the mechanisms behind thermotaxis and phototaxis, which direct a slug to a suitable site for culmination (2, 3). These model studies together with the results reported in this paper demonstrate that the entire process of morphogenesis, except for the initiation and termination of the slug stage, can unfold without any need to change the parameters of these processes. Nevertheless many genes are up- and down-regulated during slime mold development, and much more is likely to become known about the genes involved in the near future. Many of these genes are certainly connected with processes not directly related to the cell movements—e.g., the maturation of spore cells. Evaluating the role of those genes that are involved in cell movement in the light of our model should generate interesting insights into evolutionary refinements and genetic robustness and should reveal how gene expression governs macrolevel phenomena.

For example, it should be possible to interpret the aberrant phenotypes created by restriction enzyme-mediated integration (REMI) [Smith, D. (2000) Completed and near-complete 80 REMI genes (http://www-biology.ucsd.edu/others/dsmith/REMIgenes2000.html]. REMI allows both the production of mutants and the simultaneous tagging of the mutant gene. Flanking genomic sequences of significant mutants can be

recovered, cloned, and sequenced. Thus, information can be obtained about both the aberrant morphogenetic process and the gene involved, e.g., by searching for homologues. When the role of a gene at the (sub)cellular level can be elucidated, and its effect on the building blocks of our model can be determined, our modeling approach should be able to predict and explain the aberrations that can be observed during the morphogenesis. In conclusion, interpreting gene expression in terms of our model provides a heuristic method for assigning gene function in the light of the morphogenesis as a whole.

Note that our model is completely defined at the (sub)cellular level, whereas the operational units are on larger scales, ranging from individual cells to slugs, to culminants, and finally even between culminants. We have demonstrated the feasibility of such multiscale modeling for explaining the mechanisms involved in *Dictyostelium discoideum* morphogenesis. Undoubtedly, a similar approach could be adopted to unravel the mechanisms underlying other types of developmental processes (30).

We thank Dr. S. M. McNab for linguistic advice. A.F.M.M. was supported by the Priority Program Nonlinear Systems of the Netherlands Organization for Scientific Research.

1. Savill, N. J. & Hogeweg, P. (1997) *J. Theor. Biol.* **184,** 229–235.
2. Marée, A. F. M., Panfilov, A. V. & Hogeweg, P. (1999) *J. Theor. Biol.* **199,** 297–309.
3. Marée, A. F. M., Panfilov, A. V. & Hogeweg, P. (1999) *Proc. R. Soc. London Ser. B* **266,** 1351–1360.
4. Glazier, J. A. & Graner, F. (1993) *Phys. Rev. E* **47,** 2128–2154.
5. Dormann, D., Vasiev, B. & Weijer, C. J. (1998) *Biophys. Chem.* **72,** 21–35.
6. Durston, A. J., Cohen, M. H., Drage, D. J., Potel, M. J., Robertson, A. & Wonio, D. (1976) *Dev. Biol.* **52,** 173–180.
7. Wang, B. & Kuspa, A. (1997) *Science* **277,** 251–254.
8. Verkerke-Van Wijk, I. & Schaap, P. (1997) in *Dictyostelium*: *A Model System for Cell and Developmental Biology,* eds. Maeda, Y., Inouye, K. & Takeuchi, I. (Universal Academy Press, Tokyo), pp. 145–162.
9. Williams, J., Hopper, N., Early, A., Traynor, D., Harwood, A., Abe, T., Simon, M. N. & Véron, M. (1993) *Development (Cambridge, U.K.) Suppl.* **32,** 1–7.
10. Kitami, M. (1984) *Cytologia (Tokyo)* **49,** 257–264.
11. Fontana, D. R. (1995) in *Principles of Cell Adhesion*, eds. Richardson, P. D. & Steiner, M. (CRC, Boca Raton, FL), pp. 63–86.
12. Bozzaro, S. & Ponte, E. (1995) *Experientia* **51,** 1175–1188.
13. Wilkins, M. R. & Williams, K. L. (1995) *Experientia* **51,** 1189–1196.
14. Sternfeld, J. (1992) *Roux's Arch. Dev. Biol.* **201,** 354–363.
15. Williams, J. (1997) in *Dictyostelium: A Model System for Cell and Developmental Biology,* eds. Maeda, Y., Inouye, K. & Takeuchi, I. (Universal Academy Press, Tokyo), pp. 293–304.
16. Jermyn, K. A. & Williams, J. G. (1991) *Development (Cambridge, U.K.)* **111,** 779–787.
17. Watts, D. J. & Treffry, T. E. (1976) *J. Embryol. Exp. Morphol.* **35,** 323–333.
18. Panfilov, A. V. & Pertsov, A. M. (1984) *Dokl. Akad. Nauk SSSR* **274,** 1500–1503.
19. Siegert, F. & Weijer, C. (1989) *J. Cell Sci.* **93,** 325–335.
20. Siegert, F. & Weijer, C. J. (1992) *Proc. Natl. Acad. Sci. USA* **89,** 6433–6437.
21. Higuchi, G. & Yamada, T. (1984) *Cytologia (Tokyo)* **49,** 841–849.
22. Chen, T.-L. L., Kowalczyk, P. A., Ho, G. & Chisholm, R. L. (1995) *J. Cell Sci.* **108,** 3207–3218.
23. Thomason, P., Traynor, D. & Kay, R. (1999) *Trends Genet.* **15,** 15–19.
24. Harwood, A. J., Hopper, N. A., Simon, M.-N., Driscoll, D. M., Veron, M. & Williams, J. G. (1992) *Cell* **69,** 615–624.
25. Kitami, M. (1985) *Cytologia (Tokyo)* **50,** 109–115.
26. Chen, T.-L. L., Wolf, W. A. & Chisholm, R. L. (1998) *Development (Cambridge, U.K.)* **125,** 3895–3903.
27. Bonner, J. T., Suthers, H. B. & Odell, G. M. (1986) *Nature (London)* **323,** 630–632.
28. Feit, I. N. & Sollitto, R. B. (1987) *Differentiation* **33,** 193–196.
29. Williams, G. B., Elder, E. M. & Sussman, M. (1984) *Dev. Biol.* **105,** 377–388.
30. Hogeweg, P. (2000) *J. Theor. Biol.* **203,** 317–333.